Cell-Centered Discontinuous Galerkin discretization for two-dimensional Lagrangian hydrodynamics

François Vilar[a]

[a] *CEA CESTA, BP 2, 33 114 Le Barp, France*

Abstract

We present a cell-centered discontinuous Galerkin discretization for the two-dimensional gas dynamics equations written using the Lagrangian coordinates related to the initial configuration of the flow, on general unstructured grids. A finite element discretization of the deformation gradient tensor is performed ensuring the satisfaction of the Piola compatibility condition at the discrete level. A specific treatment of the geometry is done, using finite element functions to discretize the deformation gradient tensor. The Piola compatibility condition and the Geometric Conservation law are satisfied by construction of the scheme. The DG scheme is constructed by means of a cellwise polynomial basis of Taylor type. Numerical fluxes at cell interface are designed to enforce a local entropy inequality.

Keywords: DG schemes, Lagrangian hydrodynamics, initial configuration, Piola compatibility condition, deformation gradient tensor.

1. Introduction

The discontinuous Galerkin (DG) methods are locally conservative, stable and high-order accurate methods which represent one of the most promising current trends in computational fluid dynamics [2, 3]. They can be viewed as a natural high-order extension of the classical finite volume methods. This extension is constructed by means of a local variational formulation in each cell, which makes use of a piecewise polynomial approximation of the unknowns. In the present work, we describe a cell-centered DG scheme for

Email address: vilar@celia.u-bordeaux1.fr (François Vilar)

the two-dimensional system of gas dynamics equations written in the Lagrangian form, on general unstructured grids. In this particular formalism, a computational cell moves with the fluid velocity, its mass being constant, thus contact discontinuity are captured very sharply.
The aim of this work consists in extending the formalism presented in [15, 12] to the two-dimensional gas dynamics equations written using the Lagrangian coordinates related to the initial configuration of the flow. In this framework, the computational grid is fixed, however one has to follow the time evolution of the Jacobian matrix associated to the Lagrange-Euler flow map namely the gradient deformation tensor. The flow map is discretized by means of continuous mapping, using a finite element basis. This provides an approximation of the deformation gradient tensor which satisfies the Piola identity. The discretization of the physical conservation laws for the momentum and the total energy relies on a discontinuous Galerkin method. The main feature of our DG method consists in using a local Taylor basis to express the approximate solution in terms of cell averages and derivatives at cell centroids [7]. The explicit Runge-Kutta method that preserves a total variation diminishing property is employed to perform the time discretization [2]. The monotonicity is enforced by limiting the coefficients in the Taylor expansion in a hierarchical manner extending the vertex based slope limiter developed in [7, 16]. Let us note that the limitation procedure is applied using the characteristic variables projected onto the flow velocity and its orthogonal direction. We also demonstrate that our scheme, in its semi-discrete form, satisfies a global entropy inequality. This method has been developed up to the second order and its robustness and accuracy will be assessed using several relevant test cases.

2. Kinematics of fluid motion

2.1. Lagrangian and Eulerian descriptions

Let us introduce the d-dimensional Euclidean space $\mathbb{R}^d$, where d is an integer ranging from 1 to 3. Let $\mathcal{D}$ be a region of $\mathbb{R}^d$ filled by a moving fluid. The fluid flow is described mathematically by the continuous transformation, $\mathbf{\Phi}$, of $\mathcal{D}$ into itself as

$$\mathbf{\Phi} : \boldsymbol{X} \longrightarrow \boldsymbol{x} = \mathbf{\Phi}(\boldsymbol{X}, t). \tag{1}$$

Here, t, which is a non-negative real number, denotes the time and $\boldsymbol{X} = (X, Y, Z)$ is the position at time $t = 0$ of a particle moving with the fluid which

occupies the position $\boldsymbol{x}$ at time $t > 0$. By definition $\boldsymbol{\Phi}$ satisfies $\boldsymbol{\Phi}(\boldsymbol{X}, 0) = \boldsymbol{X}$. For a fixed $\boldsymbol{X}$, the time evolution of (1) describes the trajectory of a fluid particle initially located at $\boldsymbol{X}$. Let us consider $\omega = \omega(t)$ a moving sub-region of $\mathcal{D}$ at time t. The set ω corresponds to the image of a fixed sub-region Ω in the flow map with $\omega = \{\boldsymbol{x} = \boldsymbol{\Phi}(\boldsymbol{X}, t) | \boldsymbol{X} \in \Omega\}$. The boundaries of ω and Ω are respectively $\partial\omega$ and $\partial\Omega$, and their unit outward normals are $\boldsymbol{n}$ and $\boldsymbol{N}$, refer to Figure 1. At this point, we can introduce the two usual descriptions

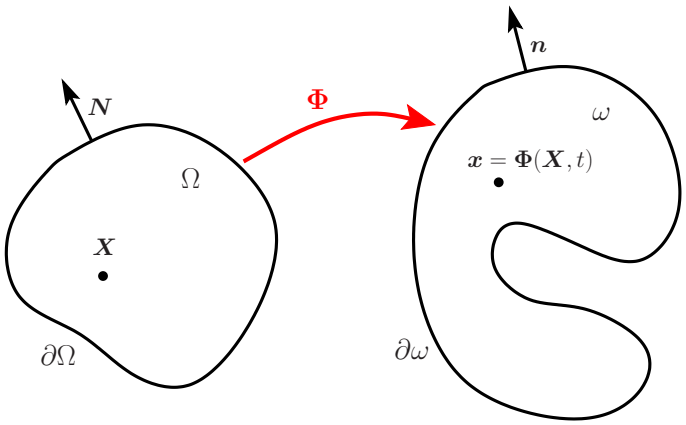

Figure 1: Notation for the flow map.

of the flows, namely the Lagrangian description and the Eulerian description. The Lagrangian description consists in observing the fluid by following the motion of fluid particles from their initial location. On the other hand the Eulerian description consists in observing the fluid at fixed locations in the space.

In the present work, we are interested by the gas dynamics equations written the Lagrangian framework

$$\rho \frac{\mathrm{d}}{\mathrm{d}t}\left(\frac{1}{\rho}\right) - \nabla_x \cdot \boldsymbol{U} = 0, \tag{2a}$$

$$\rho \frac{\mathrm{d}\,\boldsymbol{U}}{\mathrm{d}t} + \nabla_x P = \boldsymbol{0}, \tag{2b}$$

$$\rho \frac{\mathrm{d}\,E}{\mathrm{d}t} + \nabla_x \cdot (P\boldsymbol{U}) = 0, \tag{2c}$$

where ρ is the density of the fluid, $\boldsymbol{U}$ its velocity and E its total energy. Here, $\frac{\mathrm{d}}{\mathrm{d}t}$ denotes the material time derivative. The thermodynamic closure

of this system is obtained through the use of an equation of state, which writes $P = P(\rho, \varepsilon)$ where ε is the specific internal energy, $\varepsilon = E - \frac{1}{2}\boldsymbol{U}^2$. For numerical application, we use a gamma gas law, *i.e.*, $P = \rho(\gamma - 1)\varepsilon$ where γ is the polytropic index of the gas.
We made the choice of working on the initial configuration of the flow to avoid some difficulties inherent to the moving mesh scheme, as dealing with curvilinear geometries, in the case of third order scheme. To do so, we have to express the differential operators in (2a), (2b) and (2c) in terms of Lagrangian coordinates and consequently firstly characterize more precisely the motion of the fluid.

2.2. Differential operators discretization

The Jacobian matrix is used to characterize the fluid flow. This matrix also named the deformation gradient tensor is defined in terms of the Lagrangian variables as

$$\mathsf{F} = \nabla_X \boldsymbol{\Phi} = \nabla_X \boldsymbol{x}. \tag{3}$$

To ensure that the relation between the two configurations holds, we make the fundamental assumption that this matrix is invertible and its determinant, J, satisfies $J = \det \mathsf{F} > 0$ since $\mathsf{F}(\boldsymbol{X}, 0) = \mathsf{I}_d$ where I_d denotes the identity tensor. In some extreme cases of strong shocks or vortexes, the cells may tangle or present some crossed points. In these cases, J could be negative. To correct this phenomenon, an ALE approach could be needed, but in this case not by working on the shape of the deformed cells but directly on the deformation gradient tensor properties. Let $\mathrm{d}V$ and $\mathrm{d}\boldsymbol{X}$ denote a Lagrangian volume element and an infinitesimal displacement, and $\mathrm{d}v$ and $\mathrm{d}\boldsymbol{x}$ their corresponding quantities in the Eulerian space through the transformation of the flow. These volumes and displacements can be related through the following formulas

$$\begin{aligned} \mathrm{d}v &= J\mathrm{d}V, \\ \mathrm{d}\boldsymbol{x} &= \mathsf{F}\mathrm{d}\boldsymbol{X}. \end{aligned}$$

These formulas show that the Jacobian is a measure of the volume change and the deformation gradient tensor quantifies the change of shape of infinitesimal vectors through the fluid motion.

The Nanson formula gives the relation between initial and updated infinitesimal surfaces, respectively $\mathrm{d}S$ and $\mathrm{d}s$

$$\boldsymbol{n}\mathrm{d}s = J\mathsf{F}^{-t}\boldsymbol{N}\mathrm{d}S. \tag{4}$$

This is one of the main ingredient to pass from one configuration to another, and thanks to this relation we can obtain

$$\nabla_x \cdot \boldsymbol{U} = \frac{1}{J}\nabla_X \cdot (J\mathsf{F}^{-1}\boldsymbol{U}), \tag{5}$$

$$\nabla_x P = \frac{1}{J}\nabla_X \cdot (P\, J\mathsf{F}^{-t}). \tag{6}$$

At this time, it is possible to develop our system equations expressed with respect to the Lagrangian coordinates, written using the initial configuration of the flow

$$\frac{\mathrm{d}}{\mathrm{d}t}(\rho J) = 0, \tag{7a}$$

$$\rho^0 \frac{\mathrm{d}}{\mathrm{d}t}(\frac{1}{\rho}) - \nabla_X \cdot (J\mathsf{F}^{-1}\boldsymbol{U}) = 0, \tag{7b}$$

$$\rho^0 \frac{\mathrm{d}\,\boldsymbol{U}}{\mathrm{d}t} + \nabla_X \cdot (P\, J\mathsf{F}^{-t}) = \boldsymbol{0}, \tag{7c}$$

$$\rho^0 \frac{\mathrm{d}\,E}{\mathrm{d}t} + \nabla_X \cdot (P\, J\mathsf{F}^{-1}\boldsymbol{U}) = 0. \tag{7d}$$

Working with the initial positions of fluid particles, the analysis is done on a fixed domain, the initial one. However, all the informations concerning the displacement and the deformation of the domain are contained in the terms $J\mathsf{F}^{-1}$, $J\mathsf{F}^{-t}$ and so in F the deformation gradient tensor. With the use of the trajectory equation $\frac{\mathrm{d}}{\mathrm{d}t}\boldsymbol{\Phi}(\boldsymbol{X},t) = \frac{\mathrm{d}\,x}{\mathrm{d}t} = \boldsymbol{U}(\boldsymbol{X},t)$, the definition (3) yields

$$\frac{\mathrm{d}\,\mathsf{F}}{\mathrm{d}t} = \nabla_X \boldsymbol{U}. \tag{8}$$

The deformation gradient tensor contains all the information related to the flow map in the gas dynamics system. It helps us to pass from the initial configuration of the flow to the actual one. An essential identity is the well known Piola condition, that we can recover by developing the right-hand side of (5)

$$\nabla_x \cdot \boldsymbol{U} = \frac{1}{J}\boldsymbol{U} \cdot \big(\nabla_X \cdot (J\mathsf{F}^{-t})\big) + tr(\mathsf{F}^{-1}\nabla_X \boldsymbol{U}).$$

where tr is the trace operator.
If $\boldsymbol{U}$ is an arbitrary constant vector, the previous identity yields

$$\nabla_X \cdot (J\mathsf{F}^{-t}) = 0. \tag{9}$$

This Piola identity is well-known in continuum mechanics. It ensures the compatibility between the two configurations based on Eulerian and Lagrangian coordinates. This identity rewrites

$$\begin{aligned}\int_\Omega \nabla_X \cdot (J\mathsf{F}^{-t})\mathrm{d}V &= \int_{\partial\Omega} J\mathsf{F}^{-t}\boldsymbol{N}\mathrm{d}S \\ &= \int_{\partial\omega} \boldsymbol{n}\mathrm{d}s \ \text{ thanks to (4)} \\ &= \mathbf{0},\end{aligned}$$

meaning that the integral of the unit outward normal over a closed surface is equal to zero. This Piola compatibility condition is also essential because is equivalent to the Galilean invariance of the equations (7b), (7c) and (7d).

The continuity on the edges of the vector $J\mathsf{F}^{-t}\boldsymbol{N}$, which corresponds to to the normal in the actual configuration of the flow, is needed. Consequently, a discretization of the tensor F by means of a mapping using finite element basis has been chosen.

3. Discretization of the deformation

First, we subdivide each polygonal cell into triangles, as in Figure 2. Now, getting back to the mapping formulation, we develop $\boldsymbol{\Phi}$ on the finite element basis functions λ_p

$$\boldsymbol{\Phi}_h^c(\boldsymbol{X}, t) = \sum_p \lambda_p(\boldsymbol{X})\ \boldsymbol{\Phi}_p(t),$$

where the p points are some control points including vertices in a generic triangle $\mathcal{T}_c$ and $\boldsymbol{\Phi}_p(t) = \boldsymbol{\Phi}(\boldsymbol{X}_p, t)$ the position at time t of the control point initially located at $\boldsymbol{X}_p$. Using this continuous polynomial mapping approximation and the definition (3) of F, we regain a new expression for this tensor in the triangle $\mathcal{T}_c$

$$\mathsf{F}_c(\boldsymbol{X}, t) = \sum_p \boldsymbol{\Phi}_p(t) \otimes \nabla_X \lambda_p(\boldsymbol{X}). \tag{10}$$

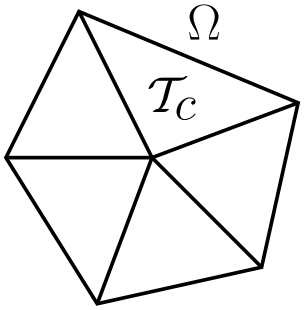

Figure 2: Triangular partitioning of a cell Ω.

Let the tensor G be the cofactor matrix of F, *i.e.*, $\mathsf{G} = J\mathsf{F}^{-t}$. The use of (10) to express G_c yields

$$\mathsf{G}_c = \begin{pmatrix} \sum_p \Phi_p^Y \partial_Y \lambda_p & -\sum_p \Phi_p^Y \partial_X \lambda_p \\ -\sum_p \Phi_p^X \partial_Y \lambda_p & \sum_p \Phi_p^X \partial_X \lambda_p \end{pmatrix} = \sum_p \begin{pmatrix} \Phi_p^Y \partial_Y \lambda_p & -\Phi_p^Y \partial_X \lambda_p \\ -\Phi_p^X \partial_Y \lambda_p & \Phi_p^X \partial_X \lambda_p \end{pmatrix}. \tag{11}$$

The compatibility between the initial and current configurations is ensured by the Piola identity. Taking the divergence of equation (11), one gets

$$\nabla_{\boldsymbol{X}} \cdot \mathsf{G}_c = \sum_p \begin{pmatrix} \Phi_p^Y (\partial_{YX} \lambda_p - \partial_{XY} \lambda_p) \\ \Phi_p^X (\partial_{XY} \lambda_p - \partial_{YX} \lambda_p) \end{pmatrix} = \mathbf{0}.$$

This equation shows that the Piola compatibility condition is satisfied by construction. This result can be generalized to three dimension with a similar procedure. Finally, as in equation (8), the use of the trajectory equation $\frac{\mathrm{d}}{\mathrm{d}t}\boldsymbol{\Phi}_p = \boldsymbol{U}_p$ leads to a semi-discrete equation of the deformation gradient tensor

$$\frac{\mathrm{d}}{\mathrm{d}t}\mathsf{F}_c(\boldsymbol{X}, t) = \sum_p \boldsymbol{U}_p(t) \otimes \nabla_X \lambda_p(\boldsymbol{X}), \tag{12}$$

where $\boldsymbol{U}_p$ is the velocity of the control point p.
Regarding (8), we make the assumption that the spatial approximation order of the deformation gradient tensor could be one less than the velocity and

so than the polynomial approximation coming from the DG discretization. Consequently, for a second order scheme, F would be piecewise constant over the triangles. For the numerical application, we use the P_1 barycentric coordinate basis functions which write

$$\lambda_p(\boldsymbol{X}) = \frac{1}{2|\mathcal{T}_c|}[X(Y_{p^+} - Y_{p^-}) - Y(X_{p^+} - X_{p^-}) + X_{p^+}Y_{p^-} - X_{p^-}Y_{p^+}], \quad (13)$$

where p, p^+ and p^- are the counterclockwise ordered triangle nodes, see Figure 3, and $|\mathcal{T}_c|$ the triangle volume.

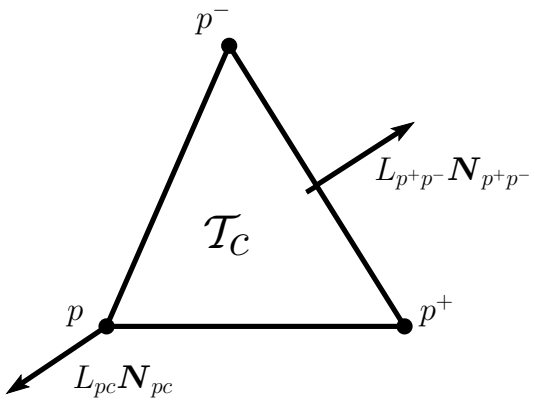

Figure 3: Generic triangle.

In this configuration, the semi-discrete equation (12) rewrites

$$\frac{\mathrm{d}}{\mathrm{d}t}\mathsf{F}_c(\boldsymbol{X}, t) = \frac{1}{|\mathcal{T}_c|}\sum_p \boldsymbol{U}_p \otimes L_{pc}\boldsymbol{N}_{pc}, \quad (14)$$

where $L_{pc}\boldsymbol{N}_{pc}$ is the corner normal at node p, as shown Figure 3, since

$$\begin{aligned}\nabla_X \lambda_p(\boldsymbol{X}) &= \frac{1}{2|\mathcal{T}_c|}\begin{pmatrix} Y_{p^+} - Y_{p^-} \\ X_{p^-} - X_{p^+} \end{pmatrix}, \\ &= \frac{1}{2|\mathcal{T}_c|}(L_{p^-p}\boldsymbol{N}_{p^-p} + L_{pp^+}\boldsymbol{N}_{pp^+}), \\ &= \frac{L_{pc}\boldsymbol{N}_{pc}}{|\mathcal{T}_c|}. \end{aligned} \quad (15)$$

Now, let us discretize the thermodynamical and kinematical equations with a discontinuous Galerkin approach.

4. Two-dimensional second order scheme

4.1. Discontinuous Galerkin system discretization

In the previous part, we discretized the deformation gradient tensor using finite element basis functions. Now, for the thermodynamical unknowns and the velocity, we present a 2D extension of the one-dimensional discontinuous Galerkin scheme presented in [15]. The method is also strongly inspired by the one developed in [9, 12, 11] and could be seen as the continuation of R. Loubère work in [8]. We develop our cell-centered DG method in the case of the two-dimensional gas dynamics system in the Lagrangian formalism based on the initial configuration of the flow.

The DG discretization can be viewed as an extension of the finite volume method wherein a piecewise polynomial approximation of the unknown is used. Let us introduce Ω our initial domain filled by a fluid, subdivided into polygonal cells Ω_c. We want to develop on each cells our unknowns onto $\mathbb{P}^{\alpha}(\Omega_c)$, the set of polynomials of degree up to α. This space approximation leads to a $(\alpha+1)^{th}$ space order accurate scheme. Let ϕ_h^c be the restriction of ϕ_h, the polynomial approximation of the function ϕ, over the cell Ω_c

$$\phi_h^c(\boldsymbol{X},t) = \sum_{k=0}^{K} \phi_k^c(t)\,\sigma_k^c(\boldsymbol{X}), \tag{16}$$

where the ϕ_k^c are the $K+1$ successive components of ϕ_h over the polynomial basis, and σ_k^c the polynomial basis functions. Recalling that the dimension of the polynomial space $\mathbb{P}^{\alpha}(\Omega_c)$ is $\frac{(\alpha+1)(\alpha+2)}{2}$, we have to determine the set of the $\frac{(\alpha+1)(\alpha+2)}{2} = K+1$ basis functions. We make the choice of the Taylor basis, which comes from a Taylor expansion on the cell, located at the center of mass $\boldsymbol{X}_c$ of the cell Ω_c defined as following

$$\boldsymbol{X}_c = \frac{1}{m_c}\int_{\Omega_c} \rho^0(\boldsymbol{X})\,\boldsymbol{X}\,\mathrm{d}\Omega, \tag{17}$$

where m_c is the constant mass of the cell Ω_c.

We set the first basis element to 1, *i.e.*, $\sigma_0^c = 1$. Going further in space discretization, the $q+1$ basis functions of degree q, with $0 < q \leq \alpha$, write

$$\sigma^c_{\frac{q(q+1)}{2}+j} = \frac{1}{j!(q-j)!}\left(\frac{X-X_c}{\Delta X_c}\right)^{q-j}\left(\frac{Y-Y_c}{\Delta Y_c}\right)^{j}, \tag{18}$$

where $j = 0 \dots q$, $\Delta X_c = \frac{X_{max} - X_{min}}{2}$ and $\Delta Y_c = \frac{Y_{max} - Y_{min}}{2}$ are the scaling factors with $X_{max}, Y_{max}, X_{min}, Y_{min}$ the maximum and minimum coordinates in the cell Ω_c. The starting index $\frac{q(q+1)}{2}$ in (18) corresponds to the number of polynomial basis functions of degree strictly inferior to q.
Let us introduce $\langle \phi \rangle_c$, the mean value of ϕ over the cell Ω_c averaged by the initial density

$$\langle \phi \rangle_c = \frac{1}{m_c} \int_{\Omega_c} \rho^0(\boldsymbol{X})\, \phi(\boldsymbol{X})\, \mathrm{d}\Omega. \tag{19}$$

In our polynomial discretization, we want the mass averaged value to be preserved. Consequently, we identify the first component of ϕ_h^c to $\langle \phi \rangle_c$, *i.e.*, $\phi_0^c = \langle \phi \rangle_c$. This definition leads to a particular constraint on the successive basis functions writing

$$\begin{aligned}
\phi_0^c &= \frac{1}{m_c} \int_{\Omega_c} \rho^0\, \phi_h^c\, \mathrm{d}\Omega, \\
&= \frac{1}{m_c} \sum_{k=0}^{K} \phi_k \int_{\Omega_c} \rho^0\, \sigma_k^c\, \mathrm{d}\Omega, \\
&= \phi_0^c + \sum_{k=1}^{K} \phi_k\, \frac{1}{m_c} \int_{\Omega_c} \rho^0\, \sigma_k^c\, \mathrm{d}\Omega, \\
&= \phi_0^c + \sum_{k=1}^{K} \phi_k\, \langle \sigma_k^c \rangle_c\,.
\end{aligned} \tag{20}$$

In order to respect equation (20), we impose $\langle \sigma_k^c \rangle_c = 0,\ \forall k \neq 0$. Consequently, we set a new definition of the $q+1$ basis functions of degree q, with $0 < q \leq \alpha$

$$\sigma^c_{\frac{q(q+1)}{2}+j} = \frac{1}{j!(q-j)!} \left[\left(\frac{X - X_c}{\Delta X_c} \right)^{q-j} \left(\frac{Y - Y_c}{\Delta Y_c} \right)^{j} - \left\langle \left(\frac{X - X_c}{\Delta X_c} \right)^{q-j} \left(\frac{Y - Y_c}{\Delta Y_c} \right)^{j} \right\rangle_c \right]. \tag{21}$$

For the second order scheme, $\alpha = 1$ and consequently $K = \frac{(\alpha+1)(\alpha+2)}{2} - 1 = 2$

$$\sigma_0^c = 1,\ \sigma_1^c = \frac{X - X_c}{\Delta X_c},\ \sigma_2^c = \frac{Y - Y_c}{\Delta Y_c}, \tag{22}$$

because by definition of the center of mass, $\langle X - X_c \rangle_c = 0$ and $\langle Y - Y_c \rangle_c = 0$.

We point out that the only geometry contributions presents in (21) and (22) are the center of mass position and the scaling factors. Consequently, regardless the shape of the cell is, we could use the same class of basis functions. We also note that the first moment ϕ_0 associated to the first basis element 1 is the mass averaged value of the function ϕ over the cell Ω_c. If the discretization ends here, the scheme would correspond to the finite volumes method averaged by the initial density. Going further, the successive moments can be identified as the successive derivatives of the function expressed at the center of mass of the cell. Here, to simplify the notation, we identify the functions $\frac{1}{\rho}$, $\boldsymbol{U}$, E and P to their polynomial approximation over the considered cell Ω_c, respectively $(\frac{1}{\rho})_h^c$, $\boldsymbol{U}_h^c$, E_h^c and P_h^c.

4.1.1. Volume equation discretization

To discretize the volume equation we perform a local variational formulation of the equation (7b) over the cell Ω_c

$$\begin{aligned}\int_{\Omega_c} \rho^0 \frac{\mathrm{d}}{\mathrm{d}t}(\frac{1}{\rho})\sigma_q^c \mathrm{d}\Omega &= \sum_{k=0}^{K} \frac{\mathrm{d}}{\mathrm{d}t}(\frac{1}{\rho})_k \int_{\Omega_c} \rho^0 \sigma_q^c \sigma_k^c \mathrm{d}\Omega \\ &= -\int_{\Omega_c} \boldsymbol{U} \cdot J\mathsf{F}^{-t} \nabla_{\boldsymbol{X}} \sigma_q^c \mathrm{d}\Omega + \int_{\partial\Omega_c} \overline{\boldsymbol{U}} \cdot \sigma_q^c J\mathsf{F}^{-t} \boldsymbol{N} \mathrm{d}L\end{aligned}$$

where σ_q^c is a function picked into the chosen basis $\{\sigma_k^c\}_{k=0\ldots K}$ of $\mathbb{P}^K$. Here, we can identify $\displaystyle\int_{\Omega_c} \rho^0 \sigma_q^c \sigma_k^c \mathrm{d}\Omega$ as a coefficient of the symmetric positive definite mass matrix. Recalling that $\displaystyle\int_{\Omega_c} \rho^0 \, \sigma_k^c \, \mathrm{d}\Omega = 0 \ \forall k \neq 0$, the equation corresponding to mass averaged value is independent of the other polynomial basis components equations.

For the second order scheme the deformation gradient tensor F and so G are constant over the triangles $\mathcal{T}_i^c$ and $\nabla_{\boldsymbol{X}} \sigma_q^c$ over Ω_c. Here, we make the assumption that the velocity on the faces surrounding a node is equal to the node velocity, *i.e.*, $\overline{\boldsymbol{U}}_{|\partial\Omega_c \cap \partial\Omega_{pc}} = \boldsymbol{U}_p$ where the Ω_{pc} are subcells of Ω_c, refer to Figure 4-(a).

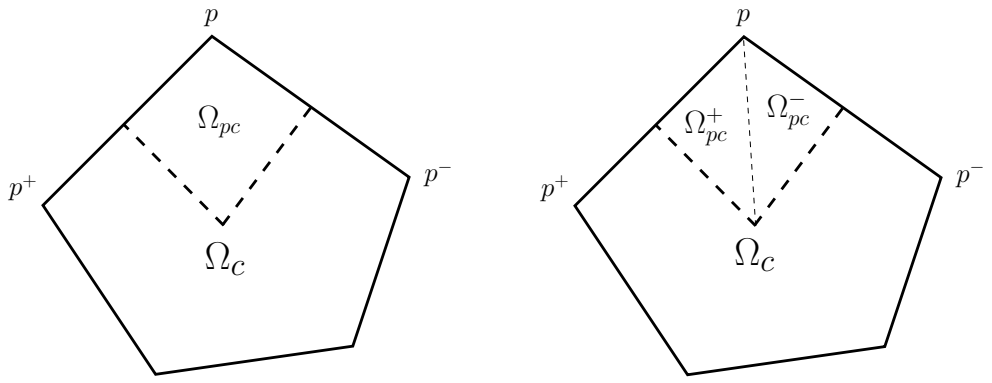

(a) Subcell Ω_{pc}. (b) Definition of $\Omega^{\pm}_{pc}$.

Figure 4: Partition of the cell Ω_c.

$$\int_{\Omega_c} \rho^0 \frac{\mathrm{d}}{\mathrm{d}t}(\frac{1}{\rho})\sigma_q^c \mathrm{d}\Omega = -\sum_{i=1}^{ntri} \mathsf{G}_i^c \nabla_{\boldsymbol{X}} \sigma_q^c \cdot \int_{\mathcal{T}_i^c} \boldsymbol{U} \mathrm{d}\mathcal{T} + \sum_{p\in\mathcal{P}(\Omega_c)} \boldsymbol{U}_p \cdot \underbrace{\int_{\partial\Omega_c\cap\partial\Omega_{pc}} \sigma_q^c \mathsf{G}\boldsymbol{N} \mathrm{d}L}_{l^q_{pc}\boldsymbol{n}^q_{pc}}$$

where $l^q_{pc}\boldsymbol{n}^q_{pc}$ denotes the q^{th} moment of the Eulerian corner normal. Finally, the equation on the specific volume leads to

$$\int_{\Omega_c} \rho^0 \frac{\mathrm{d}}{\mathrm{d}t}(\frac{1}{\rho})\sigma_q^c \mathrm{d}\Omega = -\sum_{i=1}^{ntri} \mathsf{G}_i^c \nabla_{\boldsymbol{X}} \sigma_q^c \cdot \int_{\mathcal{T}_i^c} \boldsymbol{U} \mathrm{d}\mathcal{T} + \sum_{p\in\mathcal{P}(\Omega_c)} \boldsymbol{U}_p \cdot l^q_{pc}\boldsymbol{n}^q_{pc} \tag{23}$$

For the first moment, with $l_{pc}\boldsymbol{n}_{pc} = l^0_{pc}\boldsymbol{n}^0_{pc}$, we exactly recover the EUCCLHYD scheme presented in [9, 12, 11]

$$m_c \frac{\mathrm{d}}{\mathrm{d}t}(\frac{1}{\rho})^c_0 = \sum_{p\in\mathcal{P}(\Omega_c)} \boldsymbol{U}_p \cdot l_{pc}\boldsymbol{n}_{pc}. \tag{24}$$

The scheme satisfies the GCL in the sense that the volume $|\omega_c(t)|$ of a moving cell ω_c at a time t calculated from the updated position of its nodes $\boldsymbol{x}_p$ is perfectly equivalent to the volume deriving from the volume equation discretization (24), since $\dfrac{\mathrm{d}\,|\omega_c|}{\mathrm{d}t} = \displaystyle\int_{\Omega_c} \rho^0 \frac{\mathrm{d}}{\mathrm{d}t}(\frac{1}{\rho})\mathrm{d}\Omega = m_c \frac{\mathrm{d}}{\mathrm{d}t}(\frac{1}{\rho})^c_0$.

Recalling that the volume of a generic polygonal cell writes

$$|\omega_c| = \frac{1}{2} \sum_{p \in \mathcal{P}(\Omega_c)} (\boldsymbol{x}_p \times \boldsymbol{x}_{p^+}) \cdot \boldsymbol{e}_z, \tag{25}$$

we derive a new volume equation

$$\begin{aligned}
\frac{\mathrm{d}\,|\omega_c|}{\mathrm{d}t} &= \frac{1}{2} \sum_{p \in \mathcal{P}(\Omega_c)} (\frac{\mathrm{d}\,\boldsymbol{x}_p}{\mathrm{d}t} \times \boldsymbol{x}_{p^+}) \cdot \boldsymbol{e}_z + \frac{1}{2} \sum_{p \in \mathcal{P}(\Omega_c)} (\boldsymbol{x}_p \times \frac{\mathrm{d}\,\boldsymbol{x}_{p^+}}{\mathrm{d}t}) \cdot \boldsymbol{e}_z, \\
&= \frac{1}{2} \sum_{p \in \mathcal{P}(\Omega_c)} (\boldsymbol{U}_p \times \boldsymbol{x}_{p^+}) \cdot \boldsymbol{e}_z + \frac{1}{2} \sum_{p \in \mathcal{P}(\Omega_c)} (\boldsymbol{x}_p \times \boldsymbol{U}_{p^+}) \cdot \boldsymbol{e}_z, \\
&= \frac{1}{2} \sum_{p \in \mathcal{P}(\Omega_c)} \boldsymbol{U}_p \cdot (\boldsymbol{x}_{p^+} \times \boldsymbol{e}_z) - \frac{1}{2} \sum_{p \in \mathcal{P}(\Omega_c)} \boldsymbol{U}_{p^+} \cdot (\boldsymbol{x}_p \times \boldsymbol{e}_z), \\
&= \frac{1}{2} \sum_{p \in \mathcal{P}(\Omega_c)} \boldsymbol{U}_p \cdot (\boldsymbol{x}_{p^+} \times \boldsymbol{e}_z) - \frac{1}{2} \sum_{p \in \mathcal{P}(\Omega_c)} \boldsymbol{U}_p \cdot (\boldsymbol{x}_{p^-} \times \boldsymbol{e}_z), \\
&= \sum_{p \in \mathcal{P}(\Omega_c)} \boldsymbol{U}_p \cdot \left[\left(\frac{\boldsymbol{x}_{p^+} - \boldsymbol{x}_{p^-}}{2} \right) \times \boldsymbol{e}_z \right], \\
&= \sum_{p \in \mathcal{P}(\Omega_c)} \boldsymbol{U}_p \cdot l_{pc} \boldsymbol{n}_{pc}.
\end{aligned} \tag{26}$$

The equations (26) and (24) are perfectly equivalent, consequently, the two volumes will be identical. Hence, The Geometric Conservation Law is satisfied.

4.1.2. Momentum discretization

For the momentum equation, the procedure is similar as the one presented for the volume equation. Local variational formulation of (7c) on Ω_c leads to

$$\int_{\Omega_c} \rho^0 \frac{\mathrm{d}\,\boldsymbol{U}}{\mathrm{d}t} \sigma_q^c \mathrm{d}\Omega = \sum_{i=1}^{ntri} \mathsf{G}_i^c \nabla_{\boldsymbol{X}} \sigma_q^c \int_{\mathcal{T}_i^c} P \mathrm{d}\mathcal{T} - \sum_{p \in \mathcal{P}(\Omega_c)} \boldsymbol{F}_{pc}^q \tag{27}$$

where $\boldsymbol{F}_{pc}^q = \displaystyle\int_{\partial\Omega_c \cap \partial\Omega_{pc}} \overline{P}\, \sigma_q^c \mathsf{G} \boldsymbol{N} \mathrm{d}L$ denotes the q^{th} moment of the subcell forces.

For the first moment, with $\boldsymbol{F}_{pc} = \boldsymbol{F}_{pc}^0$, we again recover the EUCCLHYD scheme

$$m_c \frac{\mathrm{d}\,\boldsymbol{U}_0^c}{\mathrm{d}t} = - \sum_{p \in \mathcal{P}(\Omega_c)} \boldsymbol{F}_{pc}. \tag{28}$$

4.1.3. Total energy discretization

Applying a local variational formulation of (7d) on Ω_c, one gets

$$\int_{\Omega_c} \rho^0 \frac{\mathrm{d}\, E}{\mathrm{d}t} \sigma_q^c \mathrm{d}\Omega = \sum_{i=1}^{ntri} \mathsf{G}_i^c \nabla_{\boldsymbol{X}} \sigma_q^c \,.\, \int_{\mathcal{T}_i^c} P\, \boldsymbol{U} \mathrm{d}\mathcal{T} - \sum_{p \in \mathcal{P}(\Omega_c)} \int_{\partial\Omega_c \cap \partial\Omega_{pc}} \overline{P\, \boldsymbol{U}} \,.\, \sigma_q^c \mathsf{G} \boldsymbol{N} \mathrm{d}L \tag{29}$$

At this point, we make the following fundamental assumption

$$\overline{P\, \boldsymbol{U}} = \overline{P}\, \overline{\boldsymbol{U}}. \tag{30}$$

With the use of the same approximation on the velocity of the faces surrounding a node, the equation on the moments of the total energy finally writes

$$\int_{\Omega_c} \rho^0 \frac{\mathrm{d}\, E}{\mathrm{d}t} \sigma_q^c \mathrm{d}\Omega = \sum_{i=1}^{ntri} \mathsf{G}_i^c \nabla_{\boldsymbol{X}} \sigma_q^c \,.\, \int_{\mathcal{T}_i^c} P\, \boldsymbol{U} \mathrm{d}\mathcal{T} - \sum_{p \in \mathcal{P}(\Omega_c)} \boldsymbol{U}_p \,.\, \boldsymbol{F}_{pc}^q \tag{31}$$

For the first moment, we can identify the EUCCLHYD scheme

$$m_c \frac{\mathrm{d}\, E_0^c}{\mathrm{d}t} = - \sum_{p \in \mathcal{P}(\Omega_c)} \boldsymbol{U}_p \,.\, \boldsymbol{F}_{pc}. \tag{32}$$

At the end, we have $3 \times (K+1)$ equations for the same number of unknowns. For $q = 0 \ldots K$

$$\sum_{k=0}^{K} \frac{\mathrm{d}}{\mathrm{d}t} (\frac{1}{\rho})_k \int_{\Omega_c} \rho^0 \sigma_q^c \sigma_k^c \mathrm{d}\Omega = - \sum_{i=1}^{ntri} \mathsf{G}_i^c \nabla_{\boldsymbol{X}} \sigma_q^c \,.\, \int_{\mathcal{T}_i^c} \boldsymbol{U} \mathrm{d}\mathcal{T} + \sum_{p \in \mathcal{P}(\Omega_c)} \boldsymbol{U}_p \,.\, l_{pc}^q \boldsymbol{n}_{pc}^q,$$

$$\sum_{k=0}^{K} \frac{\mathrm{d}\, \boldsymbol{U}_k}{\mathrm{d}t} \int_{\Omega_c} \rho^0 \sigma_q^c \sigma_k^c \mathrm{d}\Omega = \sum_{i=1}^{ntri} \mathsf{G}_i^c \nabla_{\boldsymbol{X}} \sigma_q^c \int_{\mathcal{T}_i^c} P \mathrm{d}\mathcal{T} - \sum_{p \in \mathcal{P}(\Omega_c)} \boldsymbol{F}_{pc}^q,$$

$$\sum_{k=0}^{K} \frac{\mathrm{d}\, E_k}{\mathrm{d}t} \int_{\Omega_c} \rho^0 \sigma_q^c \sigma_k^c \mathrm{d}\Omega = \sum_{i=1}^{ntri} \mathsf{G}_i^c \nabla_{\boldsymbol{X}} \sigma_q^c \,.\, \int_{\mathcal{T}_i^c} P\, \boldsymbol{U} \mathrm{d}\mathcal{T} - \sum_{p \in \mathcal{P}(\Omega_c)} \boldsymbol{U}_p \,.\, \boldsymbol{F}_{pc}^q.$$

To close the construction, we need to define our nodal solvers $\boldsymbol{U}_p$ and $\boldsymbol{F}_{pc}^q$. And as we did in the one-dimensional study presented in [15], we make an entropy analysis to ensure that the kinetic energy is correctly dissipated in internal energy through a shock.

4.2. Entropic analysis

As in the previous parts, we identify the functions $\frac{1}{\rho}$, $\boldsymbol{U}$, E and P to their polynomial approximation over the considered cell Ω_c, respectively $(\frac{1}{\rho})_h^c$, $\boldsymbol{U}_h^c$, E_h^c and P_h^c. The method is quite similar than the one used in 1D, we perform variational formulations on the gas dynamics equations (7b),(7c) and (7d) with respectively P, $\boldsymbol{U}$ and 1 as test functions

$$\int_{\Omega_c} \rho^0 \, P \frac{d}{dt}(\frac{1}{\rho}) \mathrm{d}\Omega = \int_{\partial\Omega_c} P \, \overline{\boldsymbol{U}} \,.\, J\mathsf{F}^{-t} \boldsymbol{N} \mathrm{d}L - \int_{\Omega_c} \boldsymbol{U} \,.\, J\mathsf{F}^{-t} \nabla_{\boldsymbol{X}} P \mathrm{d}\Omega, \tag{33a}$$

$$\int_{\Omega_c} \rho^0 \, \boldsymbol{U} \,.\, \frac{d\,\boldsymbol{U}}{dt} \mathrm{d}\Omega = -\int_{\partial\Omega_c} \overline{P} \, \boldsymbol{U} \,.\, J\mathsf{F}^{-t} \boldsymbol{N} \mathrm{d}L + \int_{\Omega_c} P \; tr(J\mathsf{F}^{-1} \nabla_{\boldsymbol{X}} \boldsymbol{U}) \mathrm{d}\Omega, \tag{33b}$$

$$\int_{\Omega_c} \rho^0 \frac{d\,E}{dt} \mathrm{d}\Omega = -\int_{\partial\Omega_c} \overline{P\,\boldsymbol{U}} \,.\, J\mathsf{F}^{-t} \boldsymbol{N} \mathrm{d}L. \tag{33c}$$

We identify these equations respectively to the pressure work, the kinetic energy and the total energy semi-discrete equations. Knowing that specific internal energy writes as $\varepsilon = E - \frac{1}{2}\boldsymbol{U}^2$, and specific entropy is expressed according to the Gibbs formula as $T dS = d\varepsilon + P\, d(\frac{1}{\rho})$, where T denotes the temperature, the (33c)-(33b)+(33a) combination leads to

$$\begin{aligned} \int_{\Omega_c} \rho^0 \, T \frac{d\,S}{dt} \mathrm{d}\Omega = & \int_{\partial\Omega_c} [\overline{P}\,\boldsymbol{U} + P\,\overline{\boldsymbol{U}} - \overline{P\,\boldsymbol{U}}] \,.\, J\mathsf{F}^{-t} \boldsymbol{N} \mathrm{d}L \\ & - \int_{\Omega_c} \underbrace{[P \; tr(J\mathsf{F}^{-1} \nabla_{\boldsymbol{X}} \boldsymbol{U}) + \boldsymbol{U} \,.\, J\mathsf{F}^{-t} \nabla_{\boldsymbol{X}} P]}_{\mathrm{A}} \mathrm{d}\Omega. \end{aligned}$$

The use of the Piola compatibility condition gives us

$$\begin{aligned} \nabla_{\boldsymbol{X}} \,.\, (J\mathsf{F}^{-1} P\, \boldsymbol{U}) &= \boldsymbol{U} \,.\, J\mathsf{F}^{-t} \nabla_{\boldsymbol{X}} P + P\, \nabla_{\boldsymbol{X}} \,.\, (J\mathsf{F}^{-1} \boldsymbol{U}), \\ &= \boldsymbol{U} \,.\, J\mathsf{F}^{-t} \nabla_{\boldsymbol{X}} P + P\, \boldsymbol{U} \,.\, (\underbrace{\nabla_{\boldsymbol{X}} \,.\, (J\mathsf{F}^{-t})}_{=\mathbf{0} \text{ Piola}}) + P\, tr(J\mathsf{F}^{-1} \nabla_{\boldsymbol{X}} \boldsymbol{U}), \\ &= \mathrm{A}. \end{aligned}$$

We finally get an expression of the entropy variation, recalling that $\mathsf{G} = J\mathsf{F}^{-t}$

$$\int_{\Omega_c} \rho^0 \, T \frac{d\,S}{dt} \mathrm{d}\Omega = \int_{\partial\Omega_c} [\overline{P}\,\boldsymbol{U} + P\,\overline{\boldsymbol{U}} - \overline{P\,\boldsymbol{U}} - P\,\boldsymbol{U}] \,.\, \mathsf{G}\boldsymbol{N} \mathrm{d}L, \tag{34}$$

where T denotes the temperature and S the specific entropy.
To ensure this quantity to be positive, according to the second law of thermodynamics, we set the following sufficient condition

$$\overline{P}_f(\boldsymbol{X_f}) = Pc(\boldsymbol{X_f}) - Z_c\,(\overline{\boldsymbol{U}}_f(\boldsymbol{X_f}) - \boldsymbol{U}_c(\boldsymbol{X_f}))\,.\,\frac{\mathsf{G}\boldsymbol{N}}{\|\mathsf{G}\boldsymbol{N}\|}, \tag{35}$$

where $\overline{P}_f$ and $\overline{\boldsymbol{U}}_f$ are the numerical fluxes on the face f expressed at $\boldsymbol{X}_f$, a point on it, and $P_c(\boldsymbol{X_f})$ and $\boldsymbol{U}_c(\boldsymbol{X_f})$ are the extrapolated pressure and velocity in the cell Ω_c located at this point. Z_c is a positive constant with a physical dimension of a density times a velocity.
The use of this expression to calculate $\boldsymbol{F}^q_{pc}$ leads to

$$\begin{aligned}
\boldsymbol{F}^q_{pc} &= \int_{\partial\Omega_c\cap\Omega_{pc}} \overline{P}\;\sigma^c_q \mathsf{G}\boldsymbol{N}\mathrm{d}L \\
&= \int_{\partial\Omega_c\cap\Omega_{pc}} P_c\;\sigma^c_q \mathsf{G}\boldsymbol{N}\mathrm{d}L - \int_{\partial\Omega_c\cap\Omega_{pc}} Z_c\,(\overline{\boldsymbol{U}} - \boldsymbol{U}_c)\,.\,\frac{\mathsf{G}\boldsymbol{N}}{\|\mathsf{G}\boldsymbol{N}\|}\;\sigma^c_q \mathsf{G}\boldsymbol{N}\mathrm{d}L \\
&\simeq P_c(p)\int_{\partial\Omega_c\cap\Omega_{pc}} \sigma^c_q \mathsf{G}\boldsymbol{N}\mathrm{d}L - \int_{\partial\Omega_c\cap\Omega_{pc}} Z_c\,(\boldsymbol{U}_p - \boldsymbol{U}_c(p))\,.\,\frac{\mathsf{G}\boldsymbol{N}}{\|\mathsf{G}\boldsymbol{N}\|}\;\sigma^c_q \mathsf{G}\boldsymbol{N}\mathrm{d}L \\
&= P_c(p)\,l^q_{pc}\boldsymbol{n}^q_{pc} - \mathsf{M}^q_{pc}\,(\boldsymbol{U}_p - \boldsymbol{U}_c(p)),
\end{aligned} \tag{36}$$

where the M^q_{pc} matrices are define as following

$$\begin{aligned}
\mathsf{M}^q_{pc} &= Z_c \int_{\partial\Omega_c\cap\partial\Omega_{pc}} \frac{\mathsf{G}\boldsymbol{N}}{\|\mathsf{G}\boldsymbol{N}\|}\otimes\mathsf{G}\boldsymbol{N}\;\sigma^c_q\mathrm{d}L, \\
&= Z_c\,\left(l^{q,+}_{pc}\boldsymbol{n}^+_{pc}\otimes\boldsymbol{n}^+_{pc} + l^{q,-}_{pc}\boldsymbol{n}^-_{pc}\otimes\boldsymbol{n}^-_{pc}\right),
\end{aligned}$$

where $l^{q,\pm}_{pc} = \displaystyle\int_{\partial\Omega_c\cap\partial\Omega^{\pm}_{pc}} \sigma^c_q\mathrm{d}L$, refer to Figure 4-(b).

Total energy conservation imposes, in the simple case with no boundary contribution

$$\begin{aligned}
\sum_c m_c\frac{\mathrm{d}\,E^c_0}{\mathrm{d}t} &= -\sum_c\sum_{p\in\mathcal{P}(\Omega_c)} \boldsymbol{U}_p\,.\,\boldsymbol{F}_{pc} \\
&= \sum_{p\in\mathcal{P}(\Omega)} \boldsymbol{U}_p\,.\sum_{c\in\mathcal{C}(p)} \boldsymbol{F}_{pc} \\
&= 0,
\end{aligned}$$

where $\mathcal{C}(p)$ is the set of cells surrounding the p node. Since this result holds for any velocity field, total energy conservation writes

$$\sum_{c\in\mathcal{C}(p)} \boldsymbol{F}_{pc} = \mathbf{0}. \tag{37}$$

Thanks to this constraint, we finally have an explicit expression of the nodal velocity $\boldsymbol{U}_p$

$$(\sum_{c\in\mathcal{C}(p)} M_{pc})\,\boldsymbol{U}_p = \sum_{c\in\mathcal{C}(p)} [P_c(p)\,l_{pc}\boldsymbol{n}_{pc} + \mathsf{M}_{pc}\,\boldsymbol{U}_c(p)] \tag{38}$$

where $\mathsf{M}^0_{pc} = \mathsf{M}_{pc} = Z_c\,(l^+_{pc}\boldsymbol{n}^+_{pc}\otimes\boldsymbol{n}^+_{pc} + l^-_{pc}\boldsymbol{n}^-_{pc}\otimes\boldsymbol{n}^-_{pc})$ are semi-definite positive matrices with a physical dimension of a density times a velocity. If we take into account the boundary contribution, we would get another equation defining the nodal solver for the boundary nodes.
At the end, we get a second-order semi-discrete scheme respecting by construction the Piola compatibility condition and assuring the GCL, the momentum conservation and the total energy conservation. Finally, we apply to all these semi-discretized equations a classical second-order TVD Runge-Kutta time discretization scheme [14].

Most of the test cases presented in this article contain discontinuities. In this case, a very well-known phenomenon is the apparition of oscillations when we are working with high order schemes. To avoid this problem and so to remain monotonous, we apply slope limiters.

4.3. Characteristic variables limitation

We use an extension of the Riemann invariants limitation presented in [15] setting

$$dJ^0 = \mathrm{d}E - \boldsymbol{U}\,.\,\mathrm{d}\boldsymbol{U} + P\,\mathrm{d}(\frac{1}{\rho}), \tag{39}$$

$$dJ^1_\pm = \mathrm{d}\boldsymbol{U}\,.\,\boldsymbol{\nu}_1 \mp \rho\,C\;\mathrm{d}(\frac{1}{\rho}), \tag{40}$$

$$dJ^2_\pm = \mathrm{d}\boldsymbol{U}\,.\,\boldsymbol{\nu}_2 \mp \rho\,C\,\mathrm{d}(\frac{1}{\rho}), \tag{41}$$

the differentials of the Riemann invariants extended to the two-dimensional case where C is the sound speed and $\boldsymbol{\nu}_1$ and $\boldsymbol{\nu}_2$ are two direction vectors

to define. And following the same procedure than in [15], linearizing these quantities on each cells around the mean values in the cells yields

$$J^{0,c} = E_h^c - \boldsymbol{U}_0^c \cdot \boldsymbol{U}_h^c + P_0^c \, (\frac{1}{\rho})_h^c, \tag{42}$$

$$J_{\pm}^{1,c} = \boldsymbol{U}_h^c \cdot \boldsymbol{\nu}_1 \mp \rho_0^c \, C_0^c \, (\frac{1}{\rho})_h^c, \tag{43}$$

$$J_{\pm}^{2,c} = \boldsymbol{U}_h^c \cdot \boldsymbol{\nu}_2 \mp \rho_0^c \, C_0^c \, (\frac{1}{\rho})_h^c, \tag{44}$$

where ϕ_h^i is the polynomial approximation of ϕ on the cell Ω_c and ϕ_0^c its mean value. This procedure is equivalent to linearize the equations, on each cells, around a mean state. Applying the high-order limitation procedure presented in [7], we obtain the limiting coefficients for the Riemann invariants polynomials. Consequently, using definitions (42), (43) and (44), we recover the limiting coefficients corresponding to the system variables polynomial approximations. And concerning $\boldsymbol{\nu}_1$ and $\boldsymbol{\nu}_2$, we decided to use the velocity mean value over the cell and its orthogonal direction, *i.e.*, $\boldsymbol{\nu}_1 = \boldsymbol{U}_0^c$ and $\boldsymbol{\nu}_2 = (\boldsymbol{U}_0^c)^{\perp}$, where $a^{\perp} = (-a_y, a_x)^t$ with $a = (a_x, a_y)^t$. With this procedure, we preserve the cylindrical symmetry and avoid the apparition of most of the oscillations, refer Figure 5-(b).

5. Numerical results

To demonstrate the accuracy and the robustness of our scheme on the gas dynamics system, we have run test cases taken from the literature. During the whole calculation we are working on the fixed initial grid. However, plotting final solutions on the initial mesh, the results are difficult to analyze. Nevertheless, knowing the deformation gradient tensor everywhere and at anytime, we are able to observe the solution on the actual, deformed, mesh. For a better understanding of the results, all the problem solutions are displayed on the final mesh.

5.1. Polar Sod shock tube problem

Here, we consider the extension of the classical Sod shock tube [13] to the case of polar geometry. The present problem consists of a cylindrical shock tube of unity radius. The interface is located at $r = 0.5$. At the initial time, the states on the left and on the right sides of the interface are constant. The

left state is a high pressure fluid characterized by $(\rho_L^0, P_L^0, \boldsymbol{U}_L^0) = (1, 1, \mathbf{0})$, the right state is a low pressure fluid defined by $(\rho_R^0, P_R^0, \boldsymbol{U}_R^0) = (0.125, 0.1, \mathbf{0})$. The gamma gas law is defined by $\gamma = \frac{7}{5}$. The computational domain is defined in polar coordinates by $(r, \theta) \in [0, 1] \times [0, \frac{\pi}{4}]$. The boundary conditions are symmetric for $\theta = 0$ and $\theta = \frac{\pi}{4}$, and wall, *i.e.*, the normal velocity is set to zero, at $r = 1$. The aim of this test case is to assess the scheme accuracy and the scheme symmetry preservation ability, refer Figure 5-(a). On Figure 5-(b), we note the strong accuracy difference between the first and the second order, and that we remain monotonous.

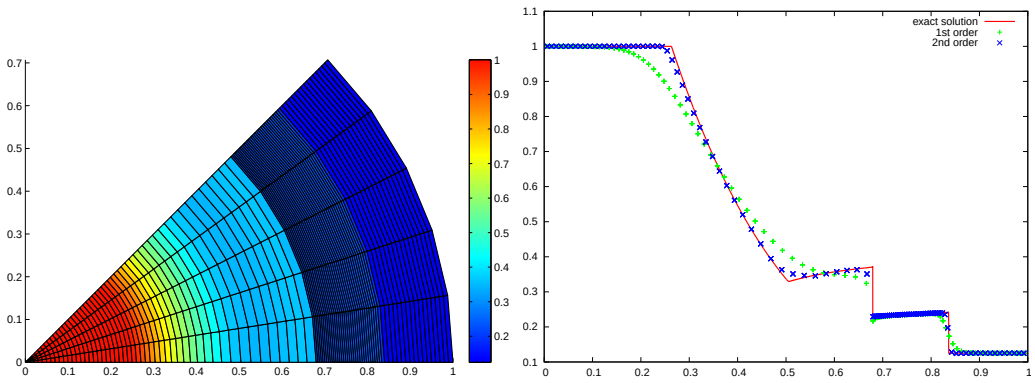

(a) Second order scheme with limitation. (b) Density profiles comparison.

Figure 5: Sod shock tube problem on a polar grid made of 100×5 cells: density map.

5.2. Noh problem

The Noh problem [10] is a famous test case used to validate Lagrangian scheme in the regime of infinite strength shock wave. In this test case, a cold gas with unit density is given an initial inward radial velocity of magnitude 1. The initial pressure is given by $P^0 = 10^{-6}$ and the polytropic index is equal to $\frac{5}{3}$. A diverging cylindrical shock wave is generated which propagates at speed $D = \dfrac{1}{3}$. The density plateau behind the shock wave reaches the value 16. The initial computational domain is defined by $(x, y) = [0, 1] \times [0, 1]$. The boundary conditions on the x and y axis are wall boundary conditions whereas a pressure given by $P^\star = P^0$ is prescribed at the outer axis $x = 1.2$ and $y = 1.2$. We run the Noh problem on a 50×50 Cartesian grid. This configuration leads to a severe test case since the mesh is not aligned with the

flow. We note we have a very smooth and cylindrical solution, and that the shock is located at a circle whose radius is approximately 0.2, refer Figure 6. On Figure 7, we observe the second order profile is very sharp at the shock wave front and very similar to the one-dimensional cylindrical solution.

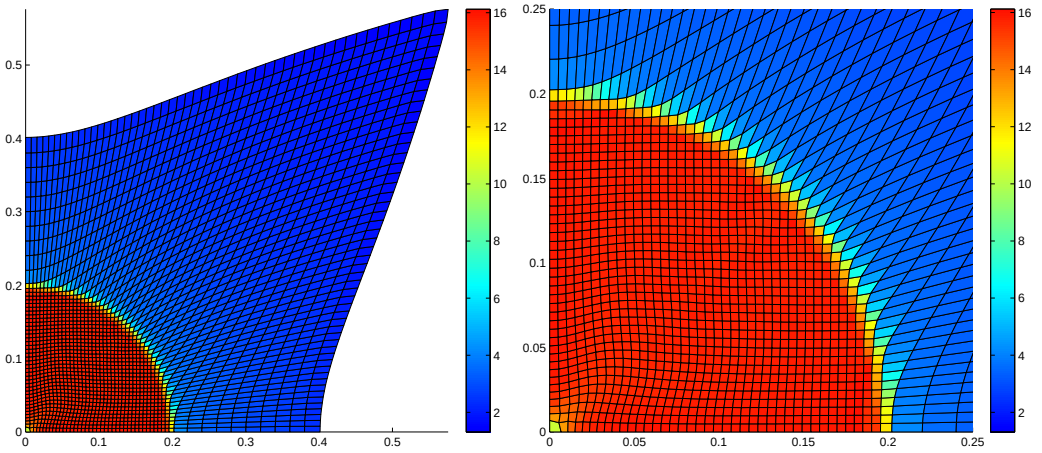

(a) Global view. (b) Zoom on the $[0, 0.25] \times [0, 0.25]$ zone.

Figure 6: Second order DG scheme with limitation for a Noh problem on a 50×50 Cartesian grid: density map.

5.3. Sedov point blast problem

We consider the Sedov problem for a point-blast in a uniform medium. An exact solution based on self-similarity arguments is available, see for instance [5]. The initial conditions are characterized by $(\rho^0, P^0, \boldsymbol{U}^0) = (1, 10^{-6}, \mathbf{0})$, and the polytropic index is equal to $\frac{7}{5}$. We set an initial delta-function energy source at the origin prescribing the pressure in the cell containing the origin as follows, $P_{or} = (\gamma - 1)\rho_{or}\dfrac{\varepsilon^0}{v_{or}}$, where v_{or} denotes the volume of the cell containing the origin and ε^0 is the total amount of release energy. By choosing $\varepsilon^0 = 0.244816$, as suggested in [5], the solution consists of a diverging infinite strength shock wave whose front is located at radius $r = 1$ at $t = 1$, with a peak density reaching 6. First, we run Sedov problem with the second order DG scheme with limitation described in this paper with a 30×30 Cartesian grid on the domain $(x, y) = [0, 1.2] \times [0, 1.2]$, refer to Figure 8-(a). Then, keeping the same conditions, we make use of an unstructured grid of 775 polygonal cells, produced by Voronoi tessellation as

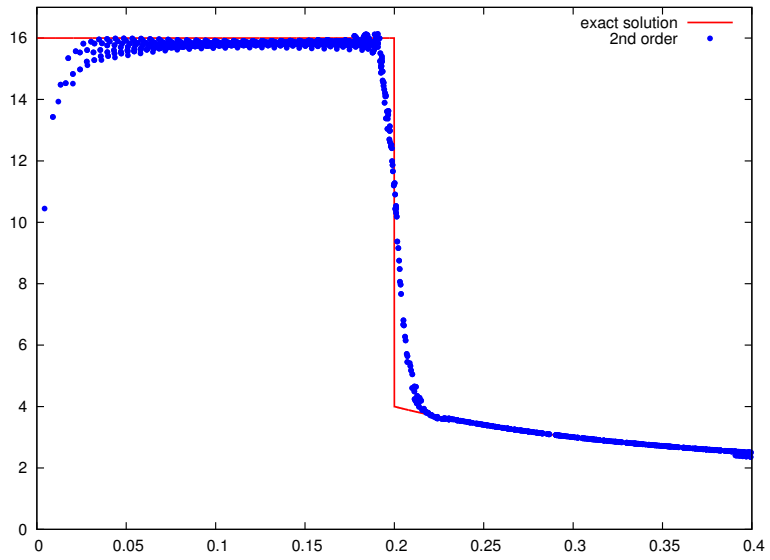

Figure 7: Density profiles comparison for a Noh problem on a 50×50 Cartesian grid.

depicts Figure 8-(b). In both cases, the shock wave front is correctly located at the end of the computation and is perfectly cylindrical, and the density peak almost reaches 6. These results demonstrate the robustness and the accuracy of this scheme.
To assess the accuracy of our DG scheme we compute the convergence order for the smooth solution of the Taylor-Green vortex test case, as in [17].

5.4. Taylor-Green vortex problem

This problem is derived by considering an analytical solution of the incompressible Navier-Stokes equations, modify to the case of compressible Euler equations. The Taylor-Green vortex is characterized by the following conditions. The computational domain is defined by $(x, y) = [0, 1] \times [0, 1]$. The initial density is uniform and denoted by ρ^0. The initial velocity field is divergence-free and reads

$$\boldsymbol{U}^0 = U^0 \begin{pmatrix} \sin(\pi x)\cos(\pi y) \\ -\cos(\pi x)\sin(\pi y) \end{pmatrix}.$$

Let us point that with these two fields, the volume equation (2a) is automatically satisfied. Now, satisfying the momentum equation (2b), P^0 is obtained

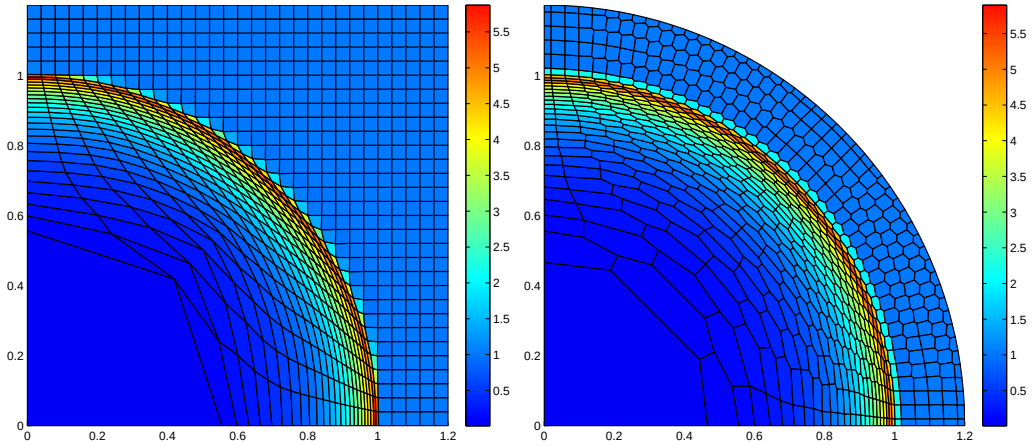

(a) On a Cartesian grid made of 900 cells. (b) On a polygonal grid made of 775 cells.

Figure 8: Second order DG scheme with limitation for a point blast Sedov problem: density map.

by balancing the inertia term as

$$\nabla_x P^0 = -\rho^0 \frac{\mathrm{d}\boldsymbol{U}^0}{\mathrm{d}t}. \tag{45}$$

After some computations, we finally obtain

$$P^0 = \frac{1}{4}\rho^0 (U^0)^2 [\cos(2\pi x) + \cos(2\pi y)] + C^0,$$

where C^0 is a constant that allows to define a non-negative pressure. Using these definitions of the density, velocity and pressure, the volume equation and the momentum equation are automatically satisfied. However, since we are computing this solution by solving the compressible Euler equations, it remains to check whether or not the energy equation (2c) is satisfied. Let us investigate first the following internal energy equation

$$\rho \frac{\mathrm{d}\,\varepsilon}{\mathrm{d}t} + P \nabla_x \cdot \boldsymbol{U} = 0, \tag{46}$$

where ε is the specific internal energy. Recalling that $\nabla_x \cdot \boldsymbol{U}^0 = 0$ and $\varepsilon^0 = \frac{P^0}{(\gamma-1)\rho^0}$, equation (46) writes initially

$$\rho^0 \frac{\mathrm{d}\,\varepsilon^0}{\mathrm{d}t} + P^0 \nabla_x \cdot \boldsymbol{U}^0 = \frac{1}{\gamma - 1} \boldsymbol{U}^0 \cdot \nabla_x P^0.$$

Replacing $\boldsymbol{U}^0$ and P^0 by their analytical expressions, we finally obtain

$$\rho^0 \frac{\mathrm{d}\,\varepsilon^0}{\mathrm{d}t} + P^0 \nabla_x \cdot \boldsymbol{U}^0 = \frac{\pi}{4} \frac{\rho^0 (U^0)^3}{\gamma - 1} [\cos(3\pi x)\cos(\pi y) - \cos(3\pi y)\cos(\pi x)]. \tag{47}$$

The following combination of the previous equations, (47) $-$ $\boldsymbol{U}^0 \cdot$ (45), leads to the total energy equation

$$\rho^0 \frac{\mathrm{d}\,E^0}{\mathrm{d}t} + \nabla_x \cdot (P^0 \boldsymbol{U}^0) = \frac{\pi}{4} \frac{\rho^0 (U^0)^3}{\gamma - 1} [\cos(3\pi x)\cos(\pi y) - \cos(3\pi y)\cos(\pi x)]. \tag{48}$$

Finally, the numerical simulation of this test case solving the Lagrangian hydrodynamics equations requires the addition of a supplementary source term in the energy (total or internal) equation.
For the numerical applications, we set $\rho^0 = 1$, $C^0 = 1$, $U^0 = 1$ and $\gamma = \frac{7}{5}$. The results displayed in Figure 9 have been obtained by our first and second order schemes on a 20×20 Cartesian grid.

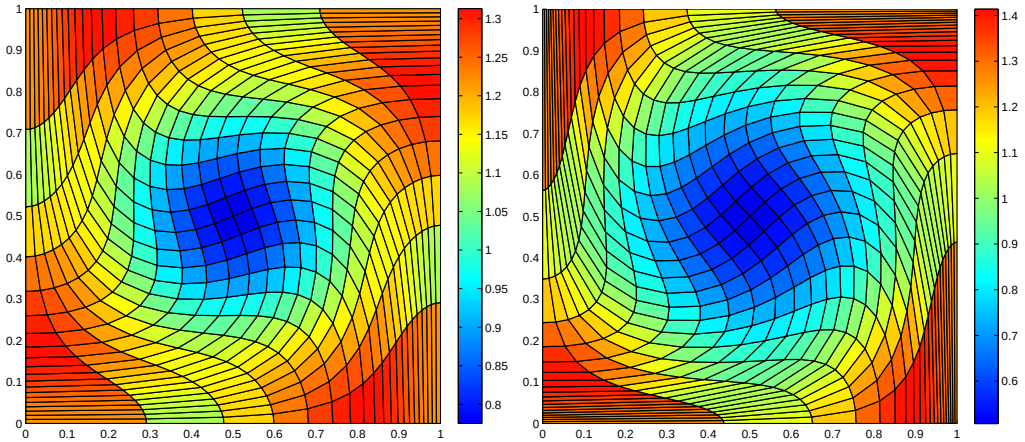

(a) First order scheme. (b) Second order scheme.

Figure 9: Taylor-Green vortex problem on a 20×20 Cartesian grid: pressure map.

Knowing the analytical solution, we can compute the numerical errors and the rate of convergence of the second order DG scheme with and without slope limiters, refer to Table 1 and Table 2.

	L_1		L_2		L_∞	
h	$E^h_{L_1}$	$q^h_{L_1}$	$E^h_{L_2}$	$q^h_{L_2}$	$E^h_{L_\infty}$	$q^h_{L_\infty}$
$\frac{1}{10}$	2.50E-2	1.48	3.71E-2	1.30	1.72E-1	1.35
$\frac{1}{20}$	8.98E-3	1.88	1.51E-2	1.75	6.73E-2	1.27
$\frac{1}{40}$	2.44E-3	1.94	4.48E-3	1.95	2.79E-2	1.68
$\frac{1}{80}$	6.36E-4	2.00	1.16E-3	2.00	8.68E-3	1.95
$\frac{1}{160}$	1.59E-4	2.01	2.90E-4	2.01	2.24E-3	2.01
$\frac{1}{320}$	3.94E-5	-	7.18E-5	-	5.54E-4	-

Table 1: rate of convergence computed on the pressure for second order DG scheme without limitation.

	L_1		L_2		L_∞	
h	$E^h_{L_1}$	$q^h_{L_1}$	$E^h_{L_2}$	$q^h_{L_2}$	$E^h_{L_\infty}$	$q^h_{L_\infty}$
$\frac{1}{10}$	5.80E-2	1.54	7.22E-2	1.31	2.24E-1	1.44
$\frac{1}{20}$	1.99E-2	2.33	2.92E-2	2.03	8.27E-2	1.34
$\frac{1}{40}$	3.96E-3	2.25	7.16E-3	2.20	3.26E-2	1.61
$\frac{1}{80}$	8.31E-4	2.17	1.56E-3	2.15	1.07E-2	1.52
$\frac{1}{160}$	1.85E-4	2.11	3.52E-4	2.14	3.73E-3	2.41
$\frac{1}{320}$	4.28E-5	-	8.01E-5	-	7.01E-4	-

Table 2: rate of convergence computed on the pressure for second order DG scheme with limitation.

We also compare these numerical errors with those obtained with another second order scheme presented in [9]. As expected, the DG scheme presented in this article is more accurate than the MUSCL scheme as show Table 3.
Another smooth problem permitting to assess the numerical accuracy of the scheme is the Kidder isentropic compression test case.

5.5. Kidder isentropic compression

In [6], Kidder has constructed an analytical solution of the self-similar isentropic compression of a shell filled with perfect gas. Following [1, 11], we recall the main features of this solution in order to define the set up of the test case. Initially, the shell has the internal (resp. external) radius R_i (resp. R_e). Let P_i, P_e, ρ_i and ρ_e be the pressures and densities located at R_i and R_e. Since the compression is isentropic, we define $s = \frac{P_e}{\rho_e^\gamma}$, and we have

	L_1		L_2		L_∞	
h	$E^h_{L_1}$	$q^h_{L_1}$	$E^h_{L_2}$	$q^h_{L_2}$	$E^h_{L_\infty}$	$q^h_{L_\infty}$
$\frac{1}{10}$	3.58E-2	1.44	5.08E-2	1.37	1.67E-1	1.17
$\frac{1}{20}$	1.32E-2	1.78	1.96E-2	1.56	7.41E-2	1.03
$\frac{1}{40}$	3.84E-3	1.93	6.66E-3	1.89	3.63E-2	1.58
$\frac{1}{80}$	1.01E-3	1.99	1.80E-3	1.98	1.21E-2	1.87
$\frac{1}{160}$	2.55E-4	2.00	4.57E-4	2.00	3.31E-3	1.97
$\frac{1}{320}$	6.38E-5	-	1.14E-4	-	8.47E-4	-

Table 3: rate of convergence computed on the pressure for second order MUSCL scheme without limitation.

$\rho_i = \rho_e \left(\frac{P_i}{P_e}\right)^{\frac{1}{\gamma}}$. Let $r(R,t)$ be the radius at time $t > 0$ of a fluid particle initially located at radius R. Looking for a solution of the gas dynamics equation under the form $r(R,t) = h(t)R$,using the isentropic feature of the flow and setting $\gamma = 1 + \frac{2}{\nu}$, where $\nu = 1, 2, 3$ indicates planar, cylindrical or spherical symmetry, we finally get the self-similar analytical solution for $t \in [0, \tau[$

$$\begin{aligned}
\rho(r(R,t),t) &= \rho^0(R)\, h(t)^{-\frac{2}{\gamma-1}},\\
U(r(R,t),t) &= R\,\frac{\mathrm{d}\,h(t)}{\mathrm{d}t},\\
P(r(R,t),t) &= P^0(R)\, h(t)^{-\frac{2\gamma}{\gamma-1}}.
\end{aligned}$$

Here, τ denotes the focusing time of the shell which is written

$$\tau = \sqrt{\frac{\gamma-1}{2}\frac{R_e^2 - R_i^2}{a_e^2 - a_i^2}},$$

where $a^2 = s\gamma\rho^{\gamma-1}$ is the square of the isentropic sound speed. The particular form of the polytropic index enables us to get the analytical expression $h(t) = \sqrt{1 - \left(\frac{t}{\tau}\right)^2}$, which is valid for any $t \in [0, \tau[$. Note that $h(t)$ goes to zero when t goes to τ, hence τ corresponds to the collapse of the shell on itself.

for $R \in [R_i, R_e]$, the initial density and pressure, ρ^0 and P^0, are defined by

$$\rho^0(R) = \left(\frac{R_e^2 - R^2}{R_e^2 - R_i^2} \rho_i^{\gamma-1} + \frac{R^2 - R_i^2}{R_e^2 - R_i^2} \rho_e^{\gamma-1} \right)^{\frac{1}{\gamma-1}},$$
$$P^0(R) = s\,(\rho^0(R))^\gamma.$$

Note that the initial velocity is equal to zero since the shell is assumed to be initially at rest. The isentropic compression is obtained imposing the following pressure laws at the internal and external faces of the shell:

$$P(r(R_i,t),t) = P_i\,h(t)^{-\frac{2\gamma}{\gamma-1}},$$
$$P(r(R_e,t),t) = P_e\,h(t)^{-\frac{2\gamma}{\gamma-1}}.$$

We point out that the velocity field is a linear function of the radius r which is a typical property of self-similar isentropic compression.
For numerical applications, we consider the cylindrical shell characterized by $R_i = 0.9$ and $R_e = 1$. We set $P_i = 0.1$, $P_e = 10$ and $\rho_e = 10^{-2}$. Due to the cylindrical symmetry we have $\nu = 2$, hence $\gamma = 2$. The previous values lead to $\rho_i = 10^{-3}$, $s = 10^5$ and $\tau \simeq 7.265E-3$. The initial computational domain is defined in polar coordinates by $(r, \theta) \in [0.9, 1] \times [0, \frac{\pi}{2}]$.
This analytical solution is useful in order to assess the scheme accuracy and the ability of a Lagrangian scheme to properly compute a spherical isentropic compression. The result displayed in Figure 10 show the symmetry is perfectly preserved, and those in Table 4 that the correct order is reached.

	L_1		L_2		L_∞	
$N_r \times N_\theta$	$E^h_{L_1}$	$q^h_{L_1}$	$E^h_{L_2}$	$q^h_{L_2}$	$E^h_{L_\infty}$	$q^h_{L_\infty}$
10×9	3.92E-2	1.82	1.55E-1	1.89	1.22E0	1.97
20×18	1.11E-2	1.95	4.18E-2	1.97	3.12E-1	1.98
40×36	2.88E-3	1.98	1.07E-2	1.99	7.92E-2	1.99
80×72	7.28E-4	1.99	2.69E-3	2.00	2.00E-2	1.99
160×144	1.83E-4	2.00	6.74E-4	2.00	5.03E-3	1.99
320×288	4.58E-5	-	1.69E-4	-	1.27E-3	-

Table 4: rate of convergence computed on the pressure for second order MUSCL scheme without limitation, at time $t = \dfrac{\tau}{2}$.

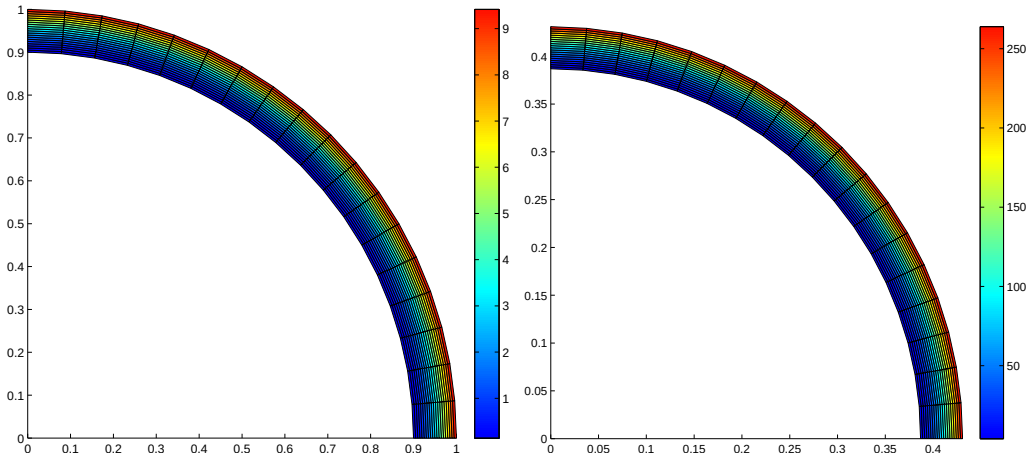

(a) At time $t = 0$. (b) At time $t = 0.9\,\tau$.

Figure 10: Second order DG scheme for a Kidder isentropic compression problem on a polar grid made of 20×18 cells: pressure map.

6. Conclusion

We have presented a cell-centered DG discretization using Taylor basis for solving two-dimensional gas dynamics equations on general unstructured grids, using the Lagrangian coordinates related to the initial configuration of the flow. In this frame, the mesh displacement and deformation are followed by the deformation gradient tensor we chose to discretize on triangles with the use of finite element basis functions. The GCL and the Piola compatibility condition are satisfied by construction of the scheme. With an analog approach to in [9], we build our nodal solvers imposing a correct entropy production and total energy conservation. Having developed properly and in a continuous manner the geometry, we can observe and display the solutions on the actual mesh. A robust and accurate limitation procedure has been constructed. The strong scheme robustness and accuracy have been assessed using several relevant test cases. In future, we plan to investigate the extension of the present DG discretization to curvilinear meshes by describing the deformation gradient tensor more precisely, and then up to the third order for the whole gas dynamics system. An extension to ALE is also scheduled.

References

[1] J. Breil, L. Hallo, P.-H. Maire and M. Olazabal-Loumé, S.-Y. Lin and C.-W. Shu, *Hydrodynamic instabilities in axisymmetric geometry self-similar models and numerical simulations.*, Laser and Particle Beams, 23:155-160,2005.

[2] B. Cockburn, S.-Y. Lin and C.-W. Shu, *TVB Runge-Kutta local projection discontinuous Galerkin finite element method for conservation laws II : one-dimensional*, J. Comp. Phys. 84:90-113, 1989.

[3] B. Cockburn, S. Hou and C.-W. Shu, *The Runge-Kutta local projection discontinuous Galerkin finite element method for conservation laws IV : the multidimensional case*, Math. Comput. 54:545-581, 1990.

[4] B. Cockburn and C.-W. Shu, *TVB Runge-Kutta local projection discontinuous Galerkin finite element method for conservation laws II : general framework*, Math. Comput. 52:411-435, 1989.

[5] J. R. Kamm and F. X. Timmes, *On efficient generation of numerically robust Sedov solutions*, Technical Report LA-UR-07-2849, Los Alamos National Laboratory, 2007.

[6] R. E. Kidder, *Laser-driven compression of hollow shells : power requirements and stability limitations*, Nucl. Fusion, 1:3-14, 1976.

[7] D. Kuzmin, *A vertex-based hierarchical slope limiter for p-adaptive discontinuous Galerkin methods*, J. Comp. Appl. Math., 233:3077-3085, 2009.

[8] R. Loubère, *Une Méthode Particulaire Lagrangienne de type Galerkin Discontinu. Application à la Mécanique des Fluides et l'Interaction Laser/Plasma*, PhD thesis, Université Bordeaux I, 2002

[9] P.-H. Maire, *A high-order cell-centered Lagrangian scheme for two-dimensional compressible fluid flows on unstructured meshes* J. Comp. Phys. 228:2391-2425, 2009.

[10] W. F. Noh, *Errors for calculations of strong shocks using artificial viscosity and an artificial heat flux* J. Comp. Phys. 72:78-120, 1987.

[11] P.-H. Maire, *Contribution to the numerical modeling of Inertial Confinement Fusion.* Habilitation à Diriger des Recherches, 2011.

[12] P.-H. Maire, *A high-order one-step sub-cell force-based discretization for cell-centered lagrangian hydrodynamics on polygonal grids.* Computers and Fluids, 2010.

[13] G. A. Sod, *A survey of several finite difference methods for systems of non-linear hyperbolic conservation laws.* , J. Comp. Phys. 27:1-31, 1978.

[14] C.-W. Shu, *Discontinuous Galerkin methods: General approach and stability*, S. Bertoluzza, S. Falletta, G. Russo and C.-W. Shu, Advanced Courses in Mathematics CRM Barcelona, Birkhäuser, Basel, 2009.

[15] F. Vilar, P.-H. Maire and R.Abgrall, *Cell-centered discontinuous Galerkin discretizations for two-dimensional scalar conservation laws on unstructured grids and for one-dimensional Lagrangian hydrodynamics.* Computers and Fluids, 46(1):498-504, 2011.

[16] M. Yang and Z.J. Wang, *A parameter- free generalized moment limiter for high-order methods on unstructured grids* Adv. Appl. Math. Mech. 1(4):451-480,2009.

[17] V. Dobrev, T. Ellis, T. Kolev and R. Rieben, *High Order Curvilinear Finite Elements for Lagrangian Hydrodynamics, Part I: General Framework*, NECDC, October 20, 2010. Available from `https://computation.llnl.gov/casc/blast/blast.html`.